Baltimore, Maryland
NOISE-CON 2010
2010 April 19-21

Planar Nearfield Acoustical Holography in High-Speed, Subsonic Flow

Yong-Joe Kim[a)]
Texas A&M University
Department of Mechanical Engineering
3123 TAMU
College Station, TX 77843-3123

Hyusang Kwon[b)]
Korea Research Institute of Standards and Science
P.O. Box 102, Yuseong
Deajon, 305-340
South Korea

The objective is to develop a NAH procedure that includes the effects of the high-speed, subsonic flow of a fluid medium. Recently, the speed of a transportation has significantly increased, e.g., to close to the speed of sound. As a result, the NAH data measured with a microphone array attached to an aircraft or train include significant airflow effects. Here, the convective wave equation along with the convective Euler's equation is used to derive the proposed NAH procedure. A mapping function between static and moving fluid medium cases is also derived from the convective wave equation. Then, a new wave number filter defined by mapping the static wave number filter is proposed. For the purpose of validating the proposed NAH procedure, a monopole simulation at Mach = -0.6 is conducted. The reconstructed acoustic fields obtained by applying the proposed NAH procedure to the simulation data match well with the exact fields. Through an experiment with two loudspeakers performed in a wind tunnel at the airflow speed of Mach = -0.12, it is also shown that the proposed NAH procedure can be used to successfully reconstruct the sound fields radiated from the two loudspeakers.

1 INTRODUCTION

Nearfield Acoustical Holography (NAH) is a powerful tool that can be used to visualize three-dimensional sound fields by projecting the sound pressure data measured on a measurement surface. The NAH procedure that includes the evanescent wave components (i.e., subsonic wave components) to improve the spatial resolution of a reconstructed sound field was first introduced by Williams et al. in 1980s.[1-3] Since then, many researchers have improved the NAH procedure and applied the improved NAH procedures to various vibro-acoustic and aeroacoustic problems.

[a)] Email address: joekim@tamu.edu
[b)] Email address: hyusang@kriss.re.kr

When the pressure data measured on a hologram surface (i.e., the measurement surface) are projected to other surfaces by using a NAH procedure, the pressure data should be spatially coherent. That is, it is required that there is only a single coherent source in the system of interest or that all measurement points in a measurement aperture are measured at the same time. The former condition is not always satisfied since the most of "real" systems have a composite source consisting of multiple incoherent noise sources. The latter condition requires a large number of microphones that completely cover a composite source although extensive research has been conducted to correctly project the sound pressure data measured only on a small patch measurement aperture.[4-8]

In order to satisfy the coherence requirement, the scan-based, multi-reference NAH procedure was introduced by Hald.[9] In this procedure, a small number of microphones is used to measure the sound pressure data on a patch of a complete hologram surface during each scanning measurement while multiple reference microphones are fixed at their locations throughout the complete scanning measurements. The measured patch data are combined to obtain complete data on the hologram surface. The combined hologram data are then decomposed into partial sound pressure fields, each is spatially coherent. Hald first proposed to use Singular Value Decomposition (SVD) to decompose the hologram data.[9] Then, each of all partial fields on the hologram surface is repetitively projected to other surfaces. The total projected fields are calculated by combining all of the projected partial fields.

The scan-based, multi-reference NAH procedure is based on the assumption that the sound field radiated from a composite source is stationary during scanning measurements. However, in a "real" NAH measurement, the sound field is not always stationary resulting in non-stationary effects. For the purpose of reducing the non-stationarity effects, a source non-stationarity compensation procedure was introduced by Kwon et al., provided that source levels are assumed to be non-stationary while their directivities remain unchanged during scanning measurements.[10]

In order to obtain physically-meaningful partial fields, it is required to place reference microphones close to noise sources.[11] Then, each of the resulting partial fields can be associated with a specific noise source. However, it is not always possible to physically place reference microphones close to noise sources. Kim et al. proposed to use virtual references of which locations are identified where beamforming powers are maximized.[11] The virtual reference procedure makes possible to identify physically-meaningful partial fields regardless of the physical locations of reference microphones.

When a NAH measurement is made with a microphone array fixed on a moving transportation means, the measured data includes the effects of the moving fluid medium such as the Doppler Effect. For example, jet noise data can be measured on the fuselage surface of a jet aircraft during its cruise condition (e.g., at Mach = 0.7) to visualize the jet noise radiated from its jet engine to fuselage surface. Another example can be the tire noise data measured with a microphone array attached to a moving vehicle. Note that the latter measurement cases can be assumed to be equivalent to the case where there is no motion with a noise source and receiver while the fluid medium is in motion with a uniform velocity. Ruhala et al. proposed a planar NAH procedure in a low-speed, moving fluid medium (e.g., below Mach = 0.1).[12] In the low-speed case, it can be assumed that a static radiation circle is shifted in the flow direction while its radius increases due to the mean flow. Thus, they proposed a wave number filter based on the shifted and expanded radiation circle. It was also assumed that the particle velocities perpendicular to the flow direction are not affected by the mean flow.

When the flow speed of a fluid medium is high and subsonic, the low-speed approximations used in the NAH procedure proposed by Ruhala et al. are no longer valid. In this article, an

improved NAH procedure is described that can be applied to the high-speed, subsonic flow conditions. In particular, a new wave number filter is proposed that is defined by mapping the static wave number filter. It is also proposed to consider the mean flow effects on the reconstructed particle velocities in the flow direction as well as in the directions perpendicular to the flow direction. Note that the proposed NAH procedure can be applied to any subsonic and uniform flow conditions regardless of low or high Mach number as long as the Mach number is within -1 to 1 range. For the purpose of validating the proposed NAH procedure, a monopole simulation at the airflow speed of Mach = -0.6 is conducted. An experiment with two loudspeakers in a wind tunnel at Mach = -0.12 is also performed.

In the following theory sections, a spatially-coherent, partial sound pressure field on a hologram surface is assumed to be given that can be obtained by using the procedures described in Refs. 10 and 11.

2 THEORY

2.1 Planar NAH in Static Fluid Medium

In order to present the proposed NAH procedure in a consistent and comprehensive manner, consider a conventional NAH procedure that can be applied to the static case where the fluid medium, composite noise source, and receiver are not in motion. When sound pressure is measured on a measurement plane at $z = z_h$ (i.e., hologram plane), the measured pressure field can be decomposed into spatially-coherent, partial sound pressure fields.[9-11] Each partial field can be then expressed as a superposition of plane wave components by applying the spatial Fourier Transform to the partial field, $p(x,y,z_h,t)$. The plane wave components (i.e., the sound pressure spectrum) in wave number domain, (k_x, k_y), can be written as

$$P(k_x, k_y, z_h, \omega) = \mathbf{F}[\, p(x, y, z_h, t)] \tag{1}$$

where **F** represents the Fourier Transform. Note that in a real implementation, the Fast Fourier Transform (FFT) is applied to spatially-sampled pressure data instead of the Fourier Transform.

The sound pressure spectrum on a reconstruction surface of $z = z_r$ can be calculated from the measured spectrum by multiplying the plane wave propagator: i.e.,

$$P(k_x, k_y, z_r, \omega) = P(k_x, k_y, z_h, \omega) K_p(k_x, k_y, z_r - z_h, \omega)\,. \tag{2}$$

In Eq. (2), K_p is the pressure propagator defined as

$$K_p(k_x, k_y, z, \omega) = \exp(ik_z z) \tag{3}$$

where

$$k_z = \begin{cases} \sqrt{k^2 - k_x^2 - k_y^2} \text{ if } k_x^2 + k_y^2 \le k^2 \\ i\sqrt{k_x^2 + k_y^2 - k^2} \text{ otherwise} \end{cases}. \tag{4}$$

In Eq. (4), k is the wave number defined as $k = \omega/c_0$ where c_0 is the speed of sound. The projected particle velocity spectrum can be obtained by applying Euler's equation into Eq. (2). Then, the velocity propagator is defined as

$$K_j(k_x, k_y, z, \omega) = \frac{k_j}{\rho_0 c_0 k} \exp(ik_z z) \ (j = x,\ y,\ \text{or } z) \tag{5}$$

where ρ_0 is the static density of the fluid medium. Thus, the projected velocity spectrum in the *j*-direction can be obtained from Eq. (2) by replacing K_p with K_j. Note that the circle with the radius of $r = k$ obtained by setting $k_z = 0$ in Eq. (4) is referred to as the radiation circle: i.e.,

$$\frac{k_x^2}{k^2} + \frac{k_y^2}{k^2} = 1. \tag{6}$$

For the plane wave components inside of the radiation circle (referred to as supersonic components), the *z*-direction wave number, k_z is a real number: i.e., the first case in Eq. (4). Thus, the propagator, K in Eq. (3) or (5) results in only phase change between two spectra at $z = z_r$ and $z = z_h$. However, when a wave component is outside of the radiation circle (that is referred to as a subsonic component), k_z is an imaginary number: i.e., the second case in Eq. (4). As a result, the propagator exponentially increases or decreases the amplitude radio of the two spectra. That is, the propagator exponentially increases the amplitude of the hologram spectrum in the case of $z_r - z_h < 0$ (i.e., backward NAH projection) while it exponentially decreases the amplitude when $z_r - z_h > 0$ (i.e., forward NAH projection). Thus, the propagator inside of the radiation circle represents a propagating wave while the propagator outside of the radiation circle represents an evanescent wave. Note that the evanescent wave applied during a backward NAH projection improves the spatial resolution of a reconstructed sound field. However, the measurement noise outside of the radiation circle is also amplified exponentially during the backward projection procedure. For the purpose of suppressing the measurement noise, it is recommended to apply the wave number filter proposed by Kwon[13] before applying the backward NAH projection (see Appendix A).

The reconstructed pressure or velocity field is obtained by applying the inverse Fourier Transform to the projected pressure or velocity spectrum: e.g.,

$$p(x, y, z_r, t) = \mathbf{F}^{-1}[P(k_x, k_y, z_r, \omega)]. \tag{7}$$

The aforementioned NAH procedure is repetitively applied to all of the partial fields on the hologram surface. The projected partial fields are then combined to obtain the total fields on the reconstruction surface. Note that sound intensity field can be calculated by multiplying the projected pressure and velocity fields.

2.2 Plane Wave Propagation in Moving Fluid Medium

Consider the (χ,ψ,ζ) coordinate system in a moving fluid medium that is corresponding to the (x,y,z) coordinate system in a static medium. When the fluid medium is moving at the uniform χ-direction velocity of U while a composite noise source and receiver are not in motion, the convective wave equation[14] can be represented as

$$\nabla^2 p = \frac{1}{c_0^2}\frac{D^2 p}{Dt^2} \tag{8}$$

where D/Dt is the total derivative (or referred to as the material derivative) that is defined as

$$\frac{D}{Dt} = \frac{\partial}{\partial t} + U\frac{\partial}{\partial \chi}. \tag{9}$$

The convective Euler's equation[14] that relates acoustic pressure and particle velocities can also be written in terms of the total derivative: i.e.,

$$\rho_0 \frac{D\vec{v}}{Dt} = -\nabla p \tag{10}$$

For the purpose of analyzing the plane wave propagation characteristics in the convective fluid medium, consider the sound pressure and particle velocity solutions represented as

$$p(\chi,\psi,\zeta,t) = P\exp[i(k_\chi\xi + k_\psi\psi + k_\zeta\zeta - \omega t)] \tag{11}$$

and

$$v_j(\chi,\psi,\zeta,t) = V_j\exp[i(k_\chi\xi + k_\psi\psi + k_\zeta\zeta - \omega t)] \tag{12}$$

where the subscript, j represents the particle velocity direction (i.e., $j = \chi$, ψ, or ζ). By applying the sound pressure solution of Eq. (11) into Eq. (8), the characteristic equation can be found as

$$k_\zeta^2 = k^2 - (1-M^2)k_\chi^2 - 2kMk_\chi - k_\psi^2 \tag{13}$$

where M is the Mach number defined as

$$M = \frac{U}{c_0}. \tag{14}$$

Similarly, by substituting Eqs. (11) and (12) into Eq. (10), the pressure and velocity can be related as

$$V_j = \frac{k_j}{\rho_0 c_0 (k - Mk_\chi)} P. \tag{15}$$

To determine a mathematical expression for the border line between supersonic and subsonic components, consider the case of $k_\zeta = 0$ in Eq. (13): i.e.,

$$\frac{\left(k_\chi + a\right)^2}{r_1^2} + \frac{k_\psi^2}{r_2^2} = 1 \tag{16}$$

where

$$a = \frac{kM}{1-M^2}, \tag{17}$$

$$r_1 = \frac{k}{1-M^2}, \tag{18}$$

and

$$r_2 = \frac{k}{\sqrt{1-M^2}}. \tag{19}$$

Eq. (16) represents an ellipse with the semimajor axis, r_1 and semiminor axis, r_2 centered at the point of ($-a$, 0). The ellipse can be referred to as the "radiation ellipse" that is corresponding to the radiation circle in the static fluid medium: i.e., the wave components inside of the radiation ellipse represent propagating waves while the outside wave components represent evanescent waves. When compared with the radiation circle shown in Eq. (6), the center of the radiation ellipse is shifted by -a along the flow direction. The radius of $r = k$ increases to r_1 in the χ-

direction and r_2 in the ψ-direction for the case of a subsonic flow (i.e., $|M| < 1$). A mapping function that maps the radiation circle in the (k_x,k_y) domain to the radiation ellipse in the (k_χ,k_ψ) domain is then defined as

$$(k_x, k_y) = \left(k(k_\chi + a)/r_1, kk_\psi / r_2\right). \tag{20}$$

The mapping of the radiation circle to the radiation ellipse is shown in Fig. 1.

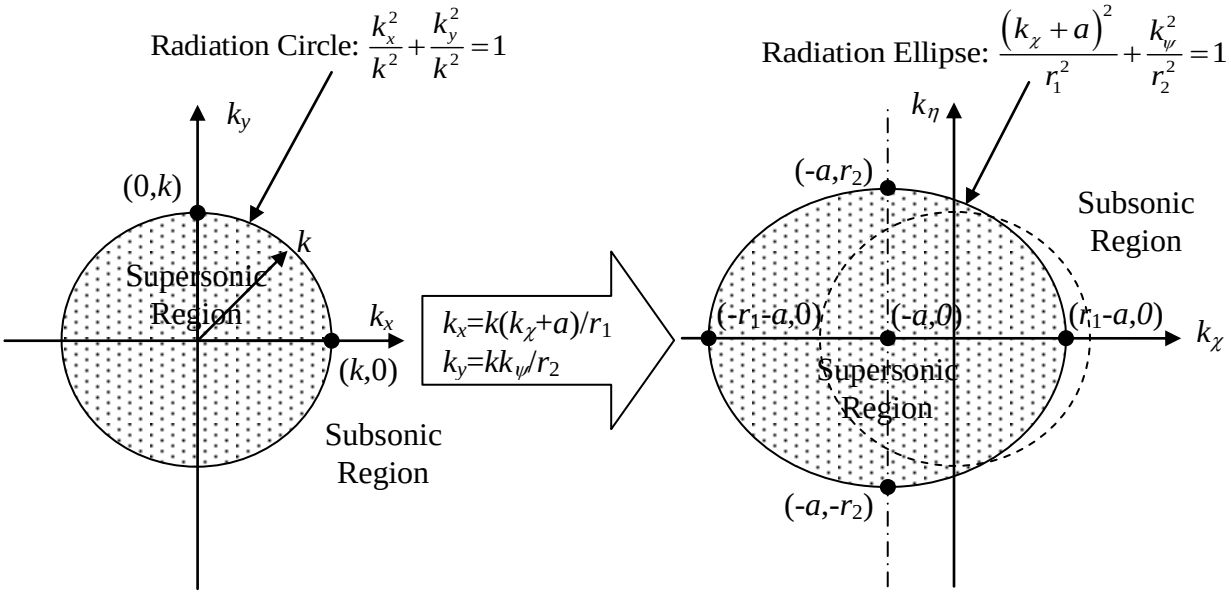

Figure 1: Mapping of radiation circle ($M = 0$) to radiation ellipse ($0 < M < 1$).

2.3 NAH Procedure in Moving Fluid Medium

When the sound pressure data are measured in the moving fluid medium, the forward and inverse Fourier Transforms given in Eqs. (1) and (7) can be re-used without any modifications. The Fourier Transforms then relate the sound pressure fields between the (χ,ψ) and (k_χ,k_ψ) domains. From Eqs. (13) and (15), the pressure and velocity propagators are defined as

$$K_p(k_\chi, k_\psi, \zeta, \omega) = \exp(ik_\zeta \zeta) \tag{21}$$

and

$$K_j(k_\chi, k_\psi, \zeta, \omega) = \frac{k_j}{\rho_0 c_0 (k - Mk_\chi)} \exp(ik_\zeta \zeta) \quad (j = \chi,\ \psi, \text{ or } \zeta) \tag{22}$$

where

$$k_\zeta = \begin{cases} \sqrt{k^2 - (1-M^2)k_\chi^2 - 2kMk_\chi - k_\psi^2} & \text{if } (1-M^2)k_\chi^2 + 2kMk_\chi + k_\psi^2 \le k^2 \\ i\sqrt{(1-M^2)k_\chi^2 + 2kMk_\chi + k_\psi^2 - k^2} & \text{otherwise} \end{cases}. \tag{23}$$

Here, a new wave number filter is proposed that is defined by mapping the static wave number filter in the (k_x,k_y) domain into the (k_χ,k_ψ) domain. By applying Eq. (20) to Eqs. (A1) - (A4) in Appendix A, the wave number filter is defined as follow:
If $k_c \geq k$,

$$W(k_\chi, k_\psi) = \begin{cases} 1-\exp[(k_r / k_c - 1)/\alpha]/2 & \text{if } k_r \leq k_c \\ \exp[(1-k_r / k_c)/\alpha]/2 & \text{otherwise} \end{cases}. \tag{24}$$

Otherwise,

$$W(k_\chi, k_\psi) = \begin{cases} 1 & \text{if } k_r \leq k \\ 0 & \text{otherwise} \end{cases} \tag{25}$$

where

$$k_r = k\sqrt{(k_\chi + a)^2 / r_1^2 + k_\psi^2 / r_2^2} \tag{26}$$

and

$$k_c = 2\pi/(3z_h) \tag{27}$$

where z_h is the hologram height.

3 MONOPOLE SIMULATION AND EXPERIMENT

For the purpose of validating the proposed NAH procedure in a moving fluid medium, the monopole simulation and experiment described in the following sections are conducted.

3.1 Simulation and Experiment Setups

The monopole simulation is set up to simulate the experiment shown in Figs. 2 and 3. An 8×5 microphone array is used for both the simulation and experiment to measure and calculate sound pressure data at each scanning position for 20 seconds at the sampling frequency of 8192 Hz. The differences between the simulation and experiment are as follow; (1) For the simulation, two uncorrelated monopole sources are placed at the locations of the two loudspeakers used in the experiment, i.e., (χ,ψ,ζ) = (0.3,0.25,-0.05) m and (0.5,0.1,-0.05) m; (2) Airflow speed is set up to M = -0.6 for the simulation while M = -0.12 for the experiment; (3) The χ-direction microphone spacing is $d\chi$ = 0.025 m in the simulation while $d\chi$ = 0.05 m in the experiment; (4) To cover the almost same measurement aperture, the total number of scans is 6 (i.e., 8×30 measurement points) in the simulation while in the experiment, the total number of scans is 3 to cover the 8×15 measurement points; (5) As shown in Figs. 2 and 3, there is a hard surface that can be assumed as a rigid boundary in the experiment while it is assumed that there is no ground condition (i.e., free field) in the simulation; (6) Input signals to the loudspeakers are directly used as reference signals in the experiment while reference signals are calculated at the locations of two reference microphones closely placed at the loudspeaker locations in the simulation; (7) A laptop with the National Instrument (NI) LabView software along with a NI 64 channel data acquisition system as shown in Fig. 3 are used to acquire sound pressure data in the experiment.

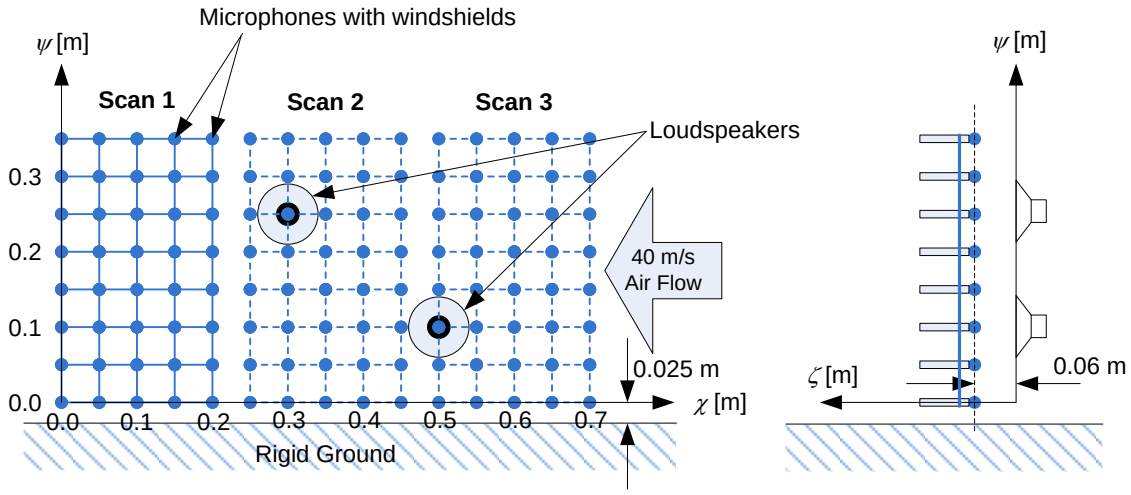

Figure 2: Sketch of experimental setup.

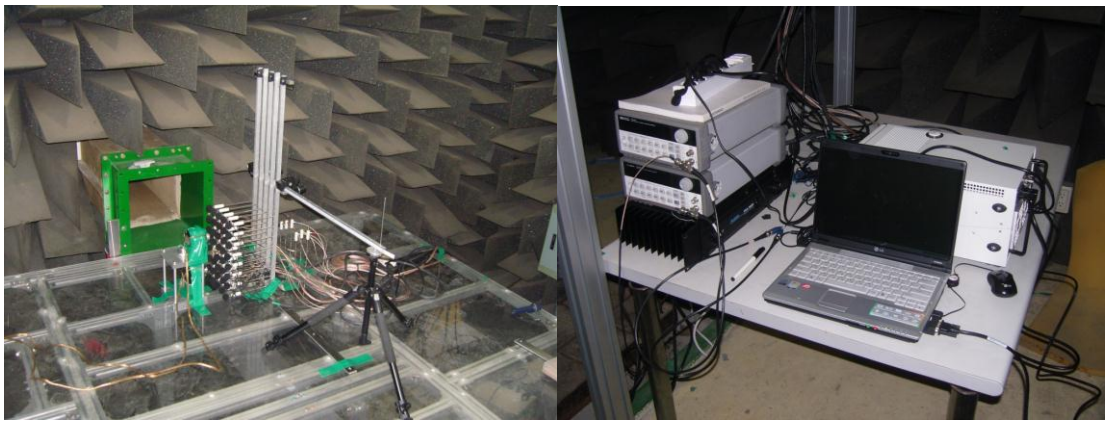

Figure 3: Photos of experimental setup.

3.2 Results and Discussion

The measured sound pressure data on the hologram surface at $\zeta = 0.06$ m are shown in Fig. 4. Figure 5 shows the imaginary part of wave number, k_ζ and the weighting function, W of the proposed wave number filter that is used for backward NAH projections when $M = -0.6$ and $f = 1.5$ kHz (see Eqs. (23) and (24)). The radiation circle in the static fluid medium case (i.e., no flow case) is overlaid as the black, solid-lined circle in Fig. 5. In Fig. 5(a), the radiation ellipse can be identified at the edge of the supersonic region where the imaginary part of k_ζ is equal to zero. Note that the center of the radiation ellipse is on the positive χ-axis due to the negative fluid flow, i.e., $M = -0.6$ (see Eqs. (16) and (17)). As you can see in Fig. 5(b), the wave number filter that is used for a backward projection passes supersonic components while it reduces the most of subsonic components with the smooth transition around the edge of the radiation ellipse.

Figure 6 shows the exact and reconstructed total sound pressure fields at $f = 1.5$ kHz. The exact sound pressure fields are shown in Figs. 6(a) and 6(b) while the reconstructed sound pressure fields presented in Figs. 6(c) and 6(d). Note the left two plots, i.e., Figs. 6(a) and 6(c) show the results at the source surface (i.e., $\zeta = 0$ m) while the right two plots, i.e., Figs. 6(b) and 6(d) show the results at the sliced surface of $\psi = 0.25$ m. As you can see, the reconstructed fields

are almost identical with the exact fields on these two surfaces except the edges of the measurement aperture (see the edges of Figs. 6(a) and 6(c)). Note that the proposed NAH projection requires that the measured sound pressure along the edges of the measurement aperture should be very small to reduce truncation errors. However, as shown in Fig. 4, the sound pressure in Fig. 4 at the top and bottom edges, in particular, at (χ,ψ) = (0.3,0.35) m and (0.5,0.0) m cannot be negligible resulting in the differences along the edges of the measurement aperture between the exact and reconstructed sound pressure fields.

Figure 7 shows the sound pressure fields on the source surface at $\zeta = 0$ that are reconstructed from experimental data when M = -0.12. As you can see, each sound pressure field represents the sound pressure field radiated from one of the loudspeakers. The locations of the highest sound pressure peaks in Fig. 7 are also in line with the locations of the loudspeakers.

4 CONCLUSIONS

In this paper, the improved NAH procedure is described that can be used to project the sound pressure data measured in a moving fluid medium with a uniform and subsonic velocity. In the latter case, a composite noise source and receiver are assumed to be not in motion. In particular, the new wave number filter is proposed that is defined by mapping the static wave number filter. The proposed velocity propagators are also recommended in order to include the mean fluid effects on reconstructed particle velocities even in the directions perpendicular to the flow direction. By applying the proposed NAH procedure to the monopole simulation data at M = -0.6, it is shown that the proposed procedure can successfully reproduce the exact sound fields. Through the experiment with the two loudspeakers performed in the wind tunnel at M = -0.12, it is also shown that the proposed NAH procedure can be used to identify the loudspeaker locations and their radiation patterns.

In the near future, it is planned to apply the proposed NAH procedure to the jet noise data measured on the fuselage surface of a jet aircraft during its cruise condition (e.g., at M = 0.7). It is also expected to develop more applications of the proposed NAH procedure in the future.

REFERENCES

1. J. D. Maynard, E. G. Williams, and Y. Lee, "Nearfield acoustic holography: I. Theory of generalized holography and the development of NAH," *Journal of Acoustical Society of America*, Vol. 78, (1985).
2. W. A. Veronesi and J. D. Maynard, "Nearfield acoustic holography (NAH): II. Holographic reconstruction algorithms and computer implementation," *Journal of Acoustical Society of America*, Vol. 81, (1985).
3. E. G. Williams, *Fourier Acoustics: Sound Radiation and Nearfield Acoustical Holography*, Academic Press, (1999).
4. J. Hald, "Patch near-field acoustical holography using a new statistically optimal method," *Proceedings of Inter-Noise 2003*, pp. 2203 – 2210, 2003.
5. J. Hald, "Patch near-field acoustical holography using a new statistically optimal method," *Brüel & Kjær Technical Review*, No. 1, pp. 44 – 54, 2005.
6. Y. T. Cho, J. S. Bolton, and J. Hald, "Source visualization by using statistically optimized near-field acoustical holography in cylindrical coordinates," *Journal of Acoustical Society of America*, Vol. 118(4), pp. 2355 – 2364, 2005.
7. E. G. Williams, "Continuation of acoustic near-fields," *Journal of Acoustical Society of America*, Vol. 113, pp.1273 – 11281, 2003.

8. M. Lee and J. S. Bolton, "Reconstruction of source distributions from sound pressures measured over discontinuous region: Multipatch holography and interpolation," *Journal of Acoustical Society of America*, Vol. 121, pp. 2086 – 2096, 2007.
9. J. Hald, "STSF – a unique technique for scan-based Nearfield acoustical holography without restriction on coherence," *Brüel & Kjær Technical Review*, No. 1, pp. 1 – 50, (1989).
10. Y.-J. Kim, J. S. Bolton, and H.-S. Kwon, "Compensation for source nonstationarity in multireference, scan-based near-field acoustical holography," *Journal of Acoustical Society of America*, Vol. 113(1), pp.360 – 368, 2003.
11. Y.-J. Kim, J. S. Bolton, and H.-S. Kwon, "Partial sound field decomposition in multireference near-field acoustical holography by using optimally located virtual references," *Journal of Acoustical Society of America*, Vol. 115(4), pp.1641 – 1652, 2004.
12. R. J. Ruhala and D. C. Swanson, "Planar near-field acoustical holography in a moving medium," *Journal of Acoustical Society of America*, Vol. 122(2), pp. 420 - 429, 2007.
13. H.-S. Kwon, *Sound visualization by using enhanced planar acoustic holographic reconstruction*, Ph.D. Thesis, Korea Advanced Institute of Science and Technologies, 1997.
14. L.E. Kinsler, A.R. Frey, A.B. Coppens, and J.V. Sanders, *Fundamentals of Acoustics*, 3rd Ed., Wiley, New York, 1982.
15. P. M. Morse and K. U. Ingard, *Theoretical Acoustics*, McGraw-Hill, Inc., 1987.

Appendix A: Wave Number Filter in Static Fluid Medium

The wave number filter proposed by Kwon[13] is presented below:
If $k_c \geq k$,

$$W(k_x, k_y) = \begin{cases} 1 - \exp[(k_r / k_c - 1)/\alpha]/2 & \text{if } k_r \leq k_c \\ \exp[(1 - k_r / k_c)/\alpha]/2 & \text{otherwise} \end{cases}. \quad \text{(A1)}$$

Otherwise,

$$W(k_x, k_y) = \begin{cases} 1 \text{ if } k_r \leq k \\ 0 \text{ otherwise} \end{cases} \quad \text{(A2)}$$

where

$$k_r = \sqrt{k_x^2 + k_y^2} \quad \text{(A3)}$$

and

$$k_c = 2\pi/(3z_h) \quad \text{(A4)}$$

where z_h is the hologram height (i.e., the distance from the source surface to measurement surface). Note that the wave number filter is the function of k_x and k_y for a given frequency (z_h is determined when the experiment is performed): i.e., k_r is the variable, and k and k_c are the constants for the given conditions.

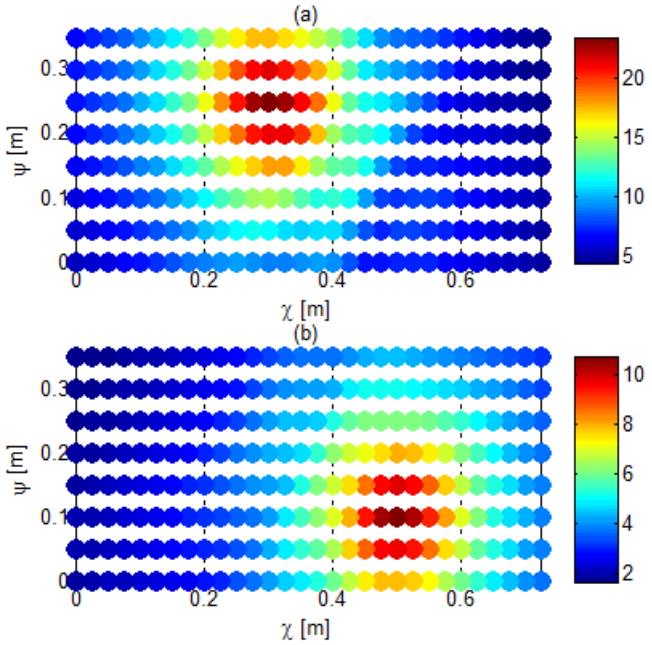

Figure 4: Measured sound pressure fields at f = 1.5 kHz on the hologram surface (monopole simulation at M = -0.6): (a) First sound pressure field and (b) Second sound pressure field.

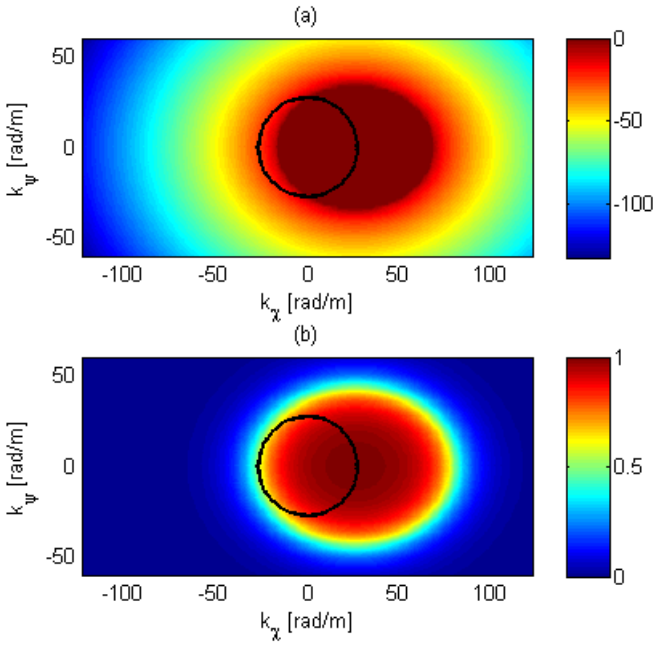

Figure 5: Two quantities in wave number domain when M = -0.6 and f = 1.5 kHz (the black, solid-lined circle represents the static radiation circle): (a) Imaginary part of wave number, k_ζ (see Eq. (23)) and (b) Weighting function, W of the proposed wave number filter (see Eq. (24)).

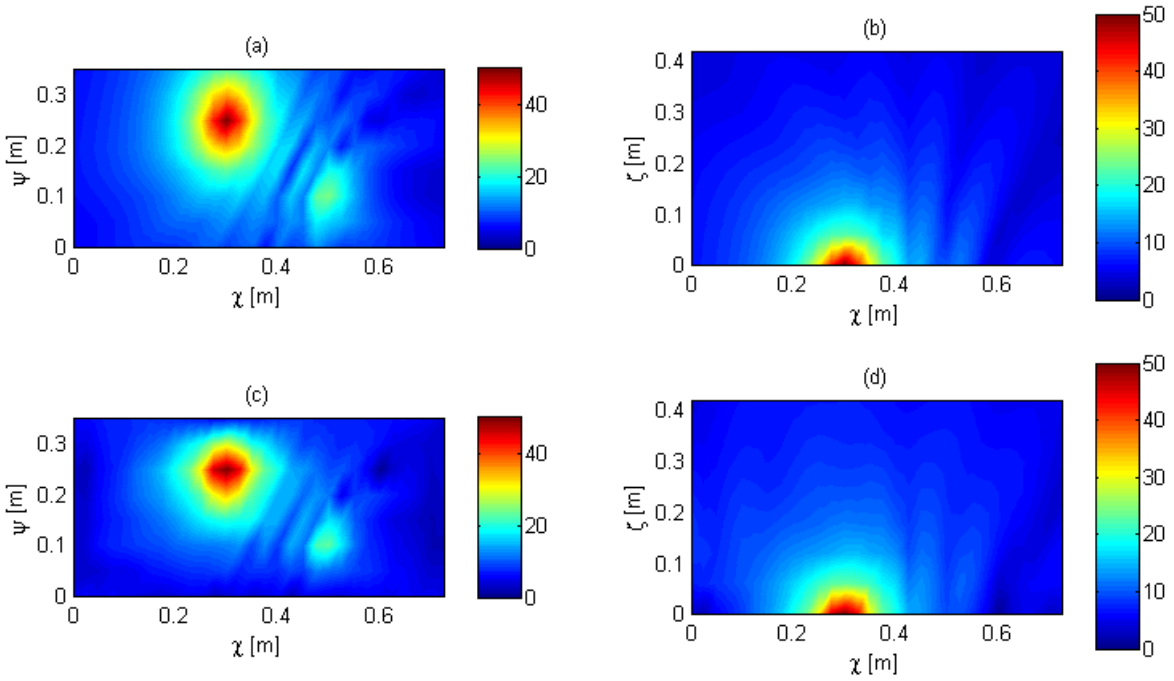

Figure 6: Total sound pressure fields at f = 1.5 kHz (monopole simulation at M = -0.6): (a) Exact sound pressure field on the surface at ζ = 0 m, (b) Exact sound pressure field on the surface at ψ = 0.25 m, (c) Reconstructed sound pressure field on the surface at ζ = 0 m, and (d) Reconstructed sound pressure field on the surface at ψ = 0.25 m.

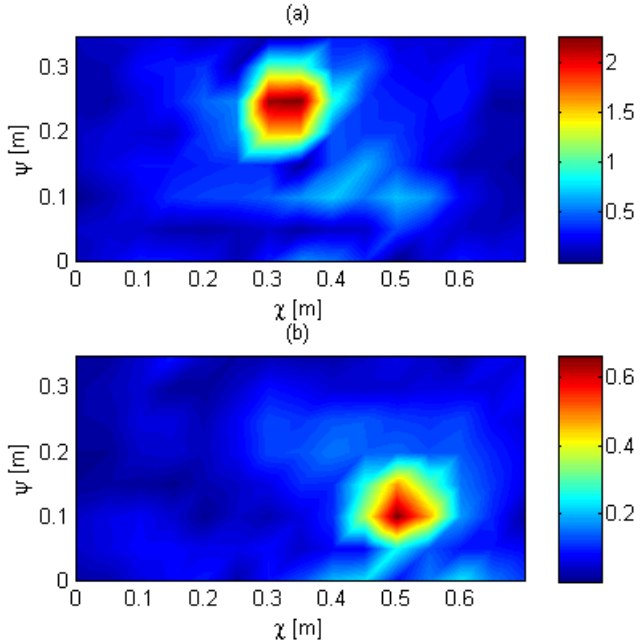

Figure 7: Reconstructed sound pressure fields on the source surface of ζ = 0 m at f = 1.5 kHz (experiment at M = -0.12): (a) First sound pressure field and (b) Second sound pressure field.